Metrol. Meas. Syst., Vol. 28 (2021) No. 2, pp. 269–288
DOI: 10.24425/mms.2021.136607

PAN POLSKA AKADEMIA NAUK

METROLOGY AND MEASUREMENT SYSTEMS
Index 330930, ISSN 0860-8229
www.metrology.wat.edu.pl

M&MS

FAULT DIAGNOSIS METHOD FOR AN AEROSPACE GENERATOR ROTATING RECTIFIER BASED ON DYNAMIC FFT TECHNOLOGY

Sai Feng, Jiang Cui, Zhuoran Zhang

Nanjing University of Aeronautics and Astronautics, College of Automation Engineering, Nanjing City, Jiangsu Province, 211100, China (*297780882@qq.com*, ✉ *cuijiang@nuaa.edu.cn*, +86 177 5177 6733, *apsc-zzr@nuaa.edu.cn*)

Abstract

A fault diagnosis method for the rotating rectifier of a brushless three-phase synchronous aerospace generator is proposed in this article. The proposed diagnostic system includes three steps: data acquisition, feature extraction and fault diagnosis. Based on a dynamic Fast Fourier Transform (FFT), this method processes the output voltages of aerospace generator continuously and monitors the continuous change trend of the main frequency in the spectrum before and after the fault. The trend can be used to perform fault diagnosis task. The fault features of the rotating rectifier proposed in this paper can quickly and effectively distinguish single and double faulty diodes. In order to verify the proposed diagnosis system, simulation and practical experiments are carried out in this paper, and good results can be achieved.

Keywords: aerospace generator, rotating rectifier, fault diagnosis, dynamic Fast Fourier Transform, feature extraction.

1. Introduction

The brushless three-phase synchronous generator, as the main electric power supplier of many airplanes, plays a very important role in the flight mission accomplishment [1]. A faulty generator can greatly threaten the safety of the overall airplane system [2]. Therefore, an automatic fault diagnosis system is necessary to monitor the technical condition of an aerospace generator and detect faults on-line. It should be able to identify the location of faults, shorten the downtime of system, and enhance the system reliability [3, 4]. Some scientists have analyzed the failure modes of brushless three-phase AC generators by discussing failure severity and the criticality number [5, 6]. The most severe failure modes of AC generator include rotating rectifier diodes faults, bearing failures, and rotor field winding faults.

In the past years, researchers have paid attention to fault detection of rectifier diodes [7–12]. These faults do not have immediate fatal consequences for the whole system, but using a generator in such a bad condition could probably result in an unexpected adverse effect on the system.

Article history: received July 17, 2020; revised November 19, 2020; accepted December 18, 2020; available online March 19, 2021.

Some approaches have been developed to diagnose an AC generator rotating rectifier, and these approaches can be divided into three categories: model-based methods, signal-based methods and pattern recognition-based methods. Model-based methods need to establish a mathematical model of the system, and the status of the system can be monitored with parameters observed for the system [5, 13]. For instance, in [14], the authors establish a model of the rotating rectifier, and give a monitoring scheme based on current analysis of the exciter. The scholars present a fault diagnosis method based on fuzzy optimization and inverse problem by studying the model of a rotating rectifier in [13]. In the applications of signal-based methods, some researchers analyse the exciter current with the Fourier transform to detect the faulty diodes [15, 16]. In [17] and [18], the scholars use output voltage of generator as the fault signal to detect faults with spectrum analysis. The pattern recognition-based method does not need a model of the system, but data analysis techniques are very important in this method. In such a method, signal from the *system under test* (SUT) needs to be collected and analysed to extract fault features. Finally, a classifier is designed to use these features for training and testing. For instance, in [19], the researchers employ a neural network as the classifier. Also in [20], the authors design a fuzzy neural network to perform fault classification of the aircraft generator.

In this article, a new fault diagnosis method for a three-phase AC generator rotating rectifier based on dynamic *Fast Fourier Transform* (FFT) technology is proposed, and this method can quickly diagnose a single diode or double diodes of the rotating rectifier. First, three-phase output voltage signals of the generator are collected, and then, the continuous change trend of the main frequency can be obtained through continuous FFT processing so as to extract effective fault features. Through the pre-set threshold value, the fault can be identified in a very short time after its occurrence. Simulated and actual experiments show that the new method has good fault detection performance under different load conditions.

2. Method presentation

2.1. Basic principle for the rotating rectifier

The three-stage brushless aerospace generator is composed of a *permanent magnet generator* (PMG), voltage regulator, exciter generator, main generator and rotating rectifier. Fig. 1 gives the typical structure of a three-stage brushless AC aerospace generator. Main function of the permanent magnet generator is to provide power for the *automatic voltage regulator* (AVR). When the generator works, the rotating rectifier rotates coaxially with the rotor of the main generator, and this can convert the three-phase alternating current generated by the exciter generator into the direct current to provide excitation for the main generator. Finally, the three-phase alternating current required is generated by the electromechanical armature of the main generator. The voltage regulator controls the excitation current of the exciter generator indirectly adjusting the excitation current of the main generator to make its output voltages stable under various working conditions.

In diagnosis application of an aerospace generator rotating rectifier, the exciter generator field current I_{ef} is the accessible signal. Main generator output voltage signal U_a, U_b and U_c changes slightly when rotating rectifier fails, and compared with I_{ef}, these signals are easier to access. Therefore, U_a, U_b and U_c are used as the fault monitoring signal of a generator rotating rectifier in this research.

Metrol. Meas. Syst., Vol. 28 (2021), No. 2, pp. 269–288
DOI: 10.24425/mms.2021.136607

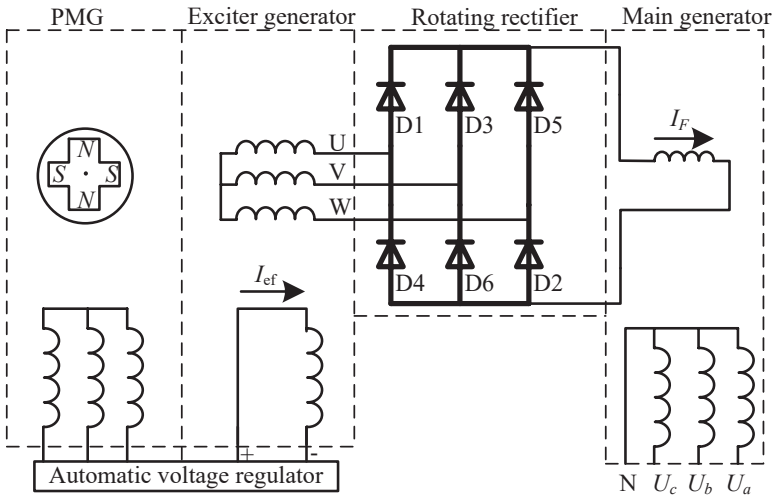

Fig. 1. The schematic diagram of AC generator.

2.2. Feature extraction based on dynamic FFT

When the AC generator works normally, the three-phase output voltages of main generator are sinusoidal periodic signals. If the rotating rectifier has an open circuit or short circuit fault, the three-phase output voltages of the main generator can be kept almost unchanged due to the feedback control of automatic voltage regulator, and they are still periodic waveforms, whose amplitudes slightly change.

This phenomenon can be seen in Fig. 2, in which, $x_p(n)$ is assumed to be the data sequence of some output voltage phase (U_a, U_b or U_c) of the main generator, and n stands for the data index for a sampled data sequence. In Fig. 2, $x_p(n)$ can be divided into $x_1(n)$ and $x_2(n)$ by the fault occurrence point. $x_1(n)$ indicates that the system works correctly, while $x_2(n)$ belongs to a faulty system.

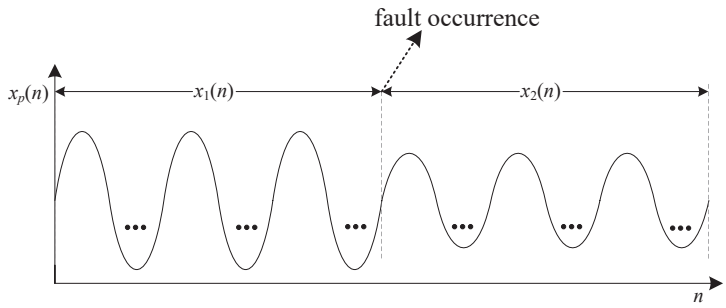

Fig. 2. System health and fault indication by $x_p(n)$.

According to the assumption above, $x_p(n)$ can be regarded as two sine sequences $x_1(n)$ and $x_2(n)$, with the same frequency and different amplitudes. Hence, this sequence can be expressed

as followed:

$$\begin{cases} x_1(n) = \begin{cases} A_1 \sin\left(n\dfrac{2\pi}{fs/f}\right), & n = 0, 1, \ldots, m-1 \\ 0, & n = m, m+1, \ldots, N-1 \end{cases} \\ x_2(n) = \begin{cases} 0, & n = 0, 1, \ldots, m-1 \\ A_2 \sin\left(n\dfrac{2\pi}{fs/f}\right), & n = m, m+1, \ldots, N-1 \end{cases} \\ x_p(n) = x_1(n) + x_2(n), \quad n = 1, 2, \ldots, N-1 \end{cases}, \tag{1}$$

where, f is the signal frequency and fs is the sampling frequency. A_1 and A_2 are positive constant values and N is the size of the whole sequence.

The mathematical expression of N points *DFT* (*Discrete Fourier Transform*) of $x_p(n)$ is as follows:

$$X_p(k) = DFT[x_p(n)] = \sum_{n=0}^{m-1} x_1(n) W_N^{nk} + \sum_{n=0}^{N-1} x_2(n) W_N^{nk} - \sum_{n=0}^{m-1} x_2(n) W_N^{nk}, \quad k = 1, 2, \ldots, N-1, \tag{2}$$

where, k is the sequence number of discrete spectral lines, $W_N = e^{-j\frac{2\pi}{N}}$.

The real part $\mathrm{Re}\, X_p(k)$ and imaginary part $\mathrm{Im}\, X_p(k)$ of the signal $x_p(n)$ after *DFT* are as follows:

$$\begin{aligned} \mathrm{Re}X_p(k) &= \sum_{n=0}^{m-1} x_1(n) \cos\left(nk\frac{2\pi}{N}\right) + \sum_{n=0}^{N-1} x_2(n) \cos\left(nk\frac{2\pi}{N}\right) - \sum_{n=0}^{m-1} x_2(n) \cos\left(nk\frac{2\pi}{N}\right), \\ &\quad k = 1, 2, \ldots, N-1, \\ \mathrm{Im}X_p(k) &= \sum_{n=0}^{m-1} x_1(n) \sin\left(nk\frac{2\pi}{N}\right) + \sum_{n=0}^{N-1} x_2(n) \sin\left(nk\frac{2\pi}{N}\right) - \sum_{n=0}^{m-1} x_2(n) \sin\left(nk\frac{2\pi}{N}\right), \\ &\quad k = 1, 2, \ldots, N-1. \end{aligned} \tag{3}$$

It can be seen from equations (2) and (3) that the spectral line $x_p(k)$ corresponding to the main frequency f will generate the peak value at the main frequency f of $x_1(n)$ and $x_2(n)$. In the case of $A_1 > A_2$ and $0 \le m \le N-1$, with m increasing from 0 to N-1, the peak value of spectral line $x_p(k)$ will increase gradually. Generally, one or more faulty diodes always result in peak value fluctuation of main frequency. This fluctuation can indicate A_2 to be smaller than A_1. In other words, by computing the change of the peak values of the main frequency, the condition of the diodes of the rectifier can be monitored.

This method, called the dynamic FFT method in our research, can be used for rotating rectifier fault feature extraction. The specific process of dynamic FFT method involves several steps as shown in Fig. 3.

(i) Collecting the output voltage signals of the main generator. Each acquisition of the output voltage is a data sample whose length is assumed to be N_1 and the time range is from t_{1s} to t_{1e}, and also, $t_{1e} = t_{1s} + N_1$.

(ii) Setting the sliding length to be L. The second data sample starts from t_{2s} and ends at t_{2e}, where $t_{2s} = t_{1s} + L$, $t_{2e} = t_{1s} + N_1 + L$; the third data sample ranges from t_{3s} to t_{3e}, where $t_{3s} = t_{1s} + 2L$, $t_{3e} = t_{1s} + N_1 + 2L$; ...; the jth data sample ranges from t_{js} to t_{je}, where $t_{js} = t_{1s} + (j-1) \times L$, $t_{je} = t_{1s} + N_1 + (j-1) \times L$.

Metrol. Meas. Syst., Vol. 28 (2021), No. 2, pp. 269–288
DOI: 10.24425/mms.2021.136607

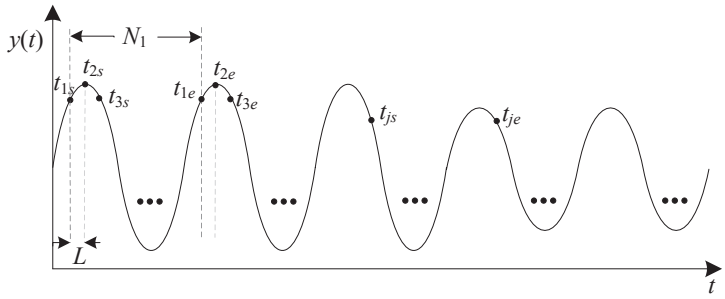

Fig. 3. Illustration of dynamic FFT processing.

(iii) Applying FFT operations to the data samples, and obtain the frequency spectral values.

In this investigation, dynamic FFT is adopted as a tool to extract features automatically, and two types of fault features of an AC generator rotating rectifier are assumed. The first is f_T feature. The specific steps of extracting f_T feature based on the dynamic FFT technology are as follows.

First, assume $x_a(t)$ to be the acquired signal of U_a and Dynamic FFT is used to process $x_a(t)$, and then absolute spectral values of $|F(\omega)|$ can be achieved. The peak value f_{pa}, corresponding to the main frequency, can be achieved with the following form:

$$f_{pa} = \max\left(|F(\omega)|\right) = \max\left(|F[x_a(t)]|\right). \tag{4}$$

Using the same method, we can get the main frequency peak values f_{pb} and f_{pc}, corresponding to U_b and U_c, respectively. In this investigation, the feature f_T is defined as:

$$f_T = \frac{f_{pa} + f_{pb} + f_{pc}}{3}. \tag{5}$$

The feature f_T can be applied to monitor fault occurrence which is demonstrated in Fig. 4. In this figure, f_T keeps unchanged before the fault (in this area, the data processed by FFT operations belongs to the "healthy" waveforms), and this feature begins to decrease after fault occurrence (entering the transition area, in which, the data processed by FFT operations belongs to both healthy and faulty waveforms), but this change becomes relatively stable after some time. In the area after the fault, the data processed with the FFT algorithm belong to the faulty waveforms.

It can be seen from Fig. 4 that the slope of f_T curve (denoted by the grey line) begins to change after fault occurrence. If the slope can be monitored, the fault can be detected sooner. Hence, inspired by the slope dynamic change of f_T feature, a second fault feature f_θ, is designed in this research. It can be derived from f_T with the following formula:

$$f_{\theta,i} = \frac{f_T(i) - f_T(i+k)}{k}, \tag{6}$$

where, k is a positive integer that should be properly selected, and i is the computation index for the features. $f_{\theta,i}$ is the ith value of feature f_θ and $f_T(i)$ is the ith value of feature f_T.

In this research, the values of f_θ appear to be a curve. Different faults can form different f_θ curves. Hence, some values on the curve can be selected as features. In our investigation, we select three values, including the maximum value of the curve and other two values around it (*i.e.* $f^*_{\theta,j-1}$ and $f^*_{\theta,j+1}$), as features. The three features are demonstrated in Fig. 4, in which, $f^*_{\theta,j}$ is the maximum value of the f_θ curve and j stands for the index of this maximum value. Three

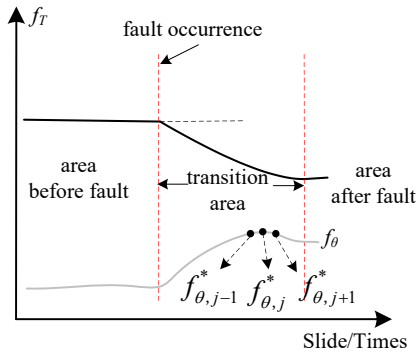

Fig. 4. Change curve of f_T before and after fault.

features, combined to be a feature sample $\left[f^*_{\theta,j-1}, f^*_{\theta,j}, f^*_{\theta,j+1}\right]$, are mainly used for the future neural classification method. In fact, other values on the f_θ curve can also be selected as the features. But we found these three features are enough to classify the fault modes.

2.3. Fault classification method

In this research, two fault classification methods are adopted for performance comparison. The first method is based on *Euclidean Distance* (ED) analysis, and the other one is the conventional *back-propagation neural network* (BPNN) method.

In the ED method, several threshold values are needed to monitor the maximum value of f_θ curve. In this study, four general faults, including working order condition, one-diode open fault, double–diode open fault and one-diode short fault, are considered. The faults can be classified with f^*_θ, which is the maximum value of the f_θ curve, according to the following formula:

$$\begin{cases} \text{health:} & f^*_\theta < ths_0 \\ \text{one-diode open fault:} & ths_0 < f^*_\theta < ths_1 \\ \text{double-diode open fault:} & ths_1 < f^*_\theta < ths_2 \\ \text{one-diode short fault:} & f^*_\theta > ths_2 \end{cases}, \tag{7}$$

where, ths_0, ths_1, and ths_2 are decision threshold values for several fault modes. These threshold values can be computed by the averaged f^*_θ for the training samples of health, one-diode open fault, double-diode open fault and one-diode short fault, respectively.

In this study, the BPNN is used because this classifier has been widely applied to fault diagnosis [21–24]. The neural network is robust to data fluctuation and noise disturbance, and more importantly, this method can learn multi-dimensional data samples. It is a good tool to perform fault classification in our applications. The basic idea of training a BPNN is the gradient steepest descent method. By using this method, the network parameters, including weights and biases, can be adjusted. The structure of the BPNN used in this study has three layers.

In this investigation, three features $\left[f^*_{\theta,j-1}, f^*_{\theta,j}, f^*_{\theta,j+1}\right]$, described in Fig. 4, are delivered to the first layer of the BPNN. The number of the third layer neurons is consistent with the number of fault modes. The activation function is also important and some previous studies can offer guidelines for constructing a proper BPNN [25]. Parameters for the BPNN in this study, including the number of the hidden layer neurons, are selected and used according to the experiment results.

3. The experiments

3.1. The first simulation experiment

3.1.1. Simulation setup

The circuit model for an AC generator is important because simulations can be conducted to pre-test the effectiveness of the algorithms. At present, the rotating rectifier of the generator uses the full bridge structure [26].

Building a model of the AC generator is complex [27]. In this paper, the model of aerospace three-stage synchronous generator (output three-phase AC voltage: 115V/400Hz, rated speed: 8000rpm) is built in MATLAB/Simulink. The overall simulation model of this aerospace generator is shown in Fig. 5.

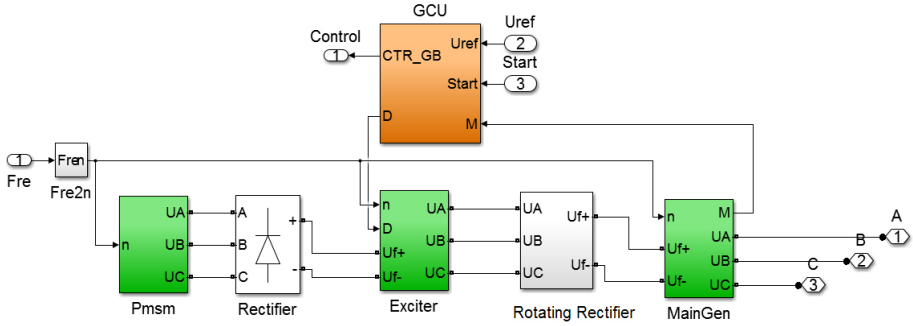

Fig. 5. The overall simulation model of an aerospace generator.

In Fig. 5, the simulation model is composed of several modules, including a *permanent magnet synchronous motor* (Pmsm), an AC exciter module (Exciter), a main generator module (MainGen) and a rotating rectifier module (Rotating Rectifier) and *generator control unit* (GCU). The rotating rectifier module is connected to the main generator whose outputs are monitored by the voltage regulator. After the output of the main generator is rectified, the voltage regulator decides whether the output meets the requirements, and then controls the excitation current of the AC exciter to indirectly adjust the excitation current of the main generator so as to adjust the output voltages [28].

Both the open-faults and the short-faults of diodes are considered in this simulation experiment. The fault modes of rotating rectifier can be divided into four types as shown in Table 1. In this table, working condition can be viewed as a special fault mode.

Table 1. Fault modes of the rotating rectifier.

Fault modes	**Specific faulty diode**
Health	–
One-Diode Open Fault	D1, D2, D3, D4, D5, D6
Double-Diode Open Fault	D1D4, D2D5, D3D6, D1D3, D1D5, D3D5 D2D4, D2D6, D4D6, D1D2, D2D3, D3D4 D4D5, D5D6, D1D6
One-Diode Short Fault	D1, D2, D3, D4, D5, D6

The model of the AC generator is simulated under three load situations (no load, resistive load and resistive-inductive load). In each load condition, the model is simulated 150 times for each fault. For each time, the data from the main generator output can be acquired from the software ports A, B and C (shown in Fig. 5), respectively. The values of loads and their tolerances are listed in Table 2.

Table 2. Parameters of different loads.

Load types	Resistance (tolerance)	Inductance (tolerance)
No load	–	–
Resistive load	30 Ω (5%)	–
Resistive-inductive load	30 Ω (5%)	500 uH (5%)

3.1.2. Data acquisition

The main generator output voltages, U_a, U_b and U_c, are collected at a sampling rate of 50 KSa/s, and each sample contains 2000 data points. For each fault mode, 150 samples are collected. Some waveforms of main generator outputs with no load are shown in Fig. 6. The output

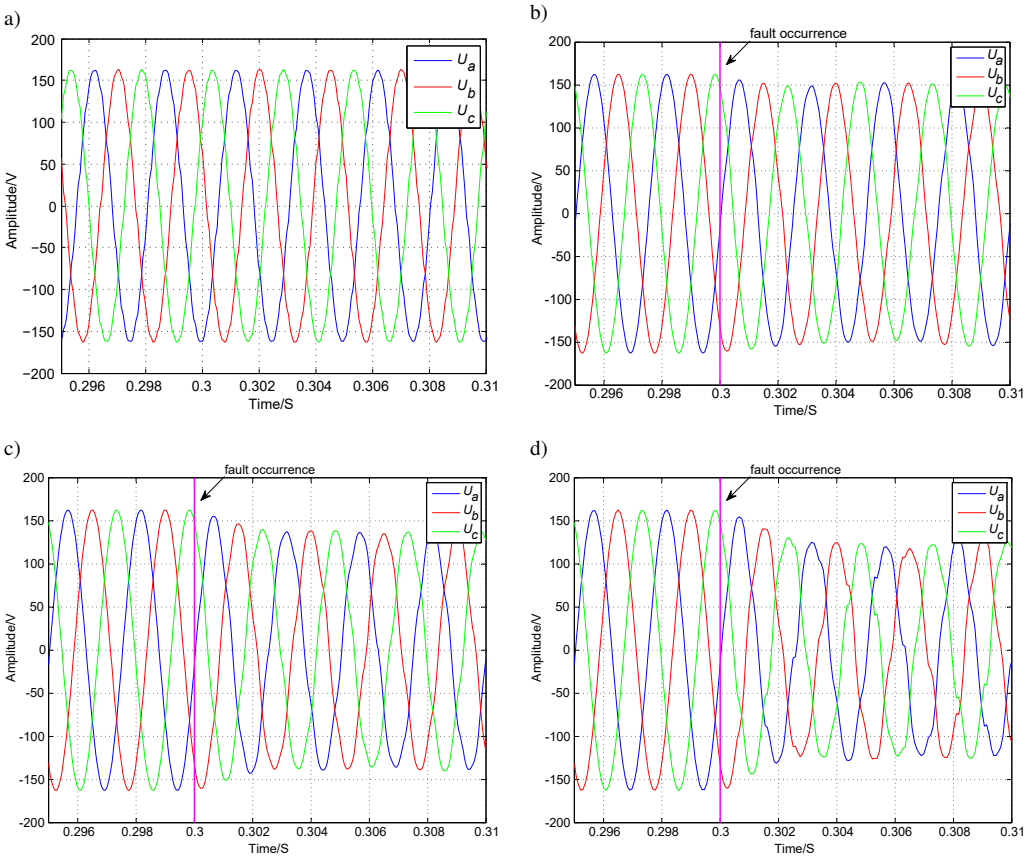

Fig. 6. Waveforms under different faults: (a) working order; (b) D1 – open fault; (c) D1D3 – open fault; (d) D1 – short fault.

voltages fall slightly when fault is triggered at 0.3 s and the fault occurrence is indicated with a vertical line in Fig. 6.

As shown in the figures above, in the case of fault occurrence, the output voltage attenuation of AC generator can be found. A similar phenomenon can be observed under the other two load conditions.

3.1.3. Feature extraction

After obtaining three-phase output voltages under several load conditions, computations of the FFT analysis on these voltage signals are carried out. The input length of the FFT is set as 256.

Under no-load condition, taking U_a as an example, the spectrum of the rotating rectifier in working order, D1 open circuit fault, D1D4 open circuit fault and D1 short circuit fault is shown in Fig. 7, respectively.

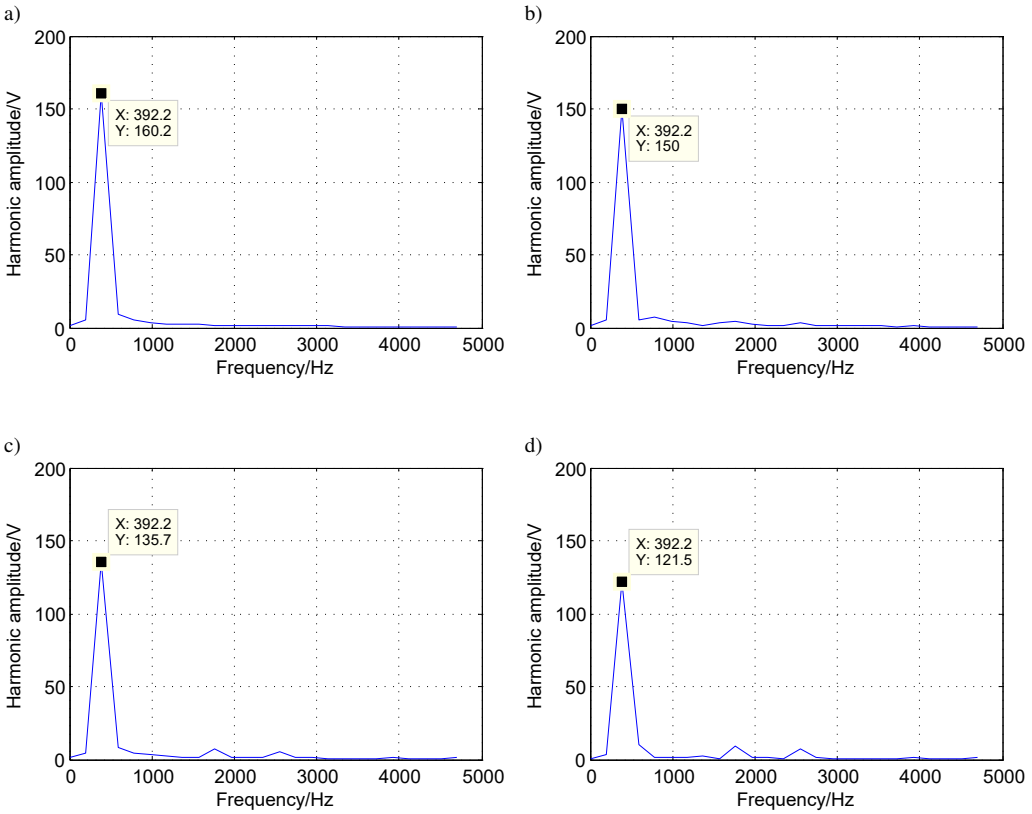

Fig. 7. Spectrum of U_a under different faults: (a) health condition; (b) D1 – open fault; (c) D1D3 – open fault; (d) D1 – short fault.

It can be seen from the spectrum that the main frequency changes slightly when the rotating rectifier is with one-diode open fault. But, the main frequency changes obviously with double-diode open fault. When the rotating rectifier is with one-diode short fault, the output voltages of the generator will decrease significantly. This shows that with increasing the number of

open circuit diodes in the rotating rectifier, the influence on the output voltage signal of the generator increases accordingly. This also shows that the short circuit fault is more dangerous than the open circuit fault. A similar phenomenon can be observed under the other two load conditions.

The dynamic FFT is performed for each sample with a fixed length of 256 points and the sliding length is set to be 5. In this way, 349 instances of sliding FFT processing are carried out, and the feature curve of f_T after each dynamic FFT can be observed in Fig. 8, under no load condition, resistive load condition and resistive-inductive load condition, respectively.

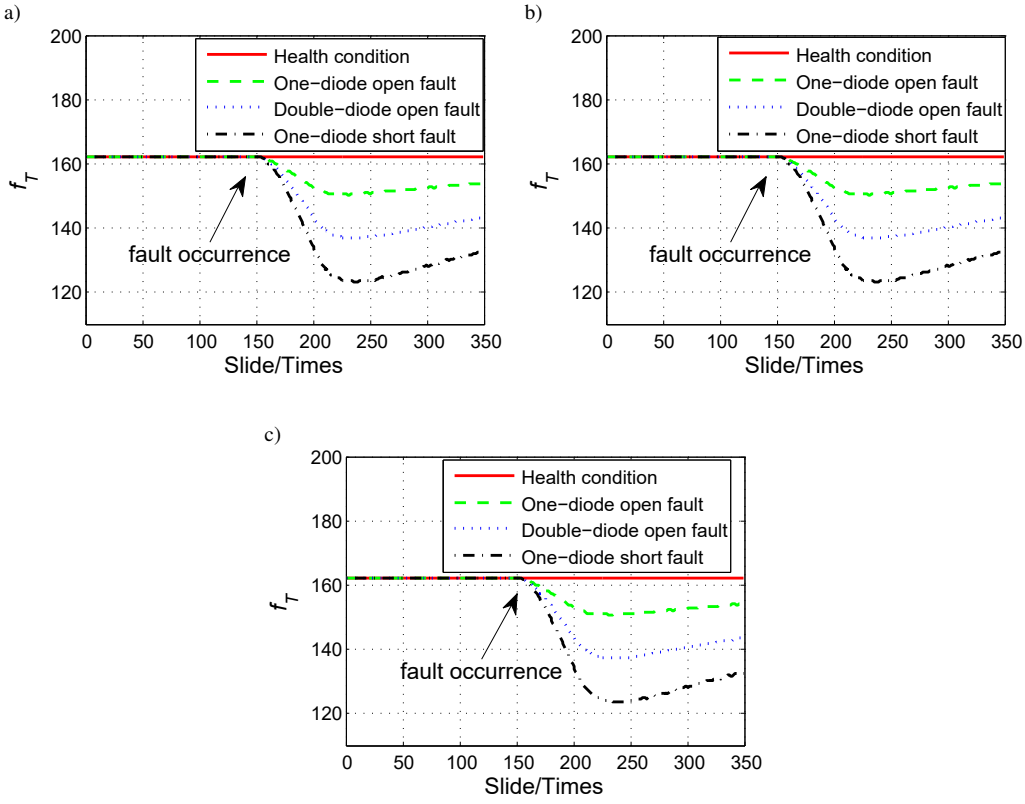

Fig. 8. Change curve of f_T under different load conditions: (a) no load condition; (b) resistive load condition; (c) resistive-inductive load condition.

It can be seen from Fig. 8 that, f_T feature curves drop sharply after the open/short fault occurrence of rotating rectifier diodes. For different faults, the change curves appear obviously different. This phenomenon exists in different loads. This shows that this phenomenon is independent of the type of load on the generator. This stratification phenomenon makes it possible to perform fault classification. Based on f_T features, f_θ feature curve can be achieved easily with formula (6) and the curves for f_θ, under different load conditions can be seen in Fig. 9, respectively.

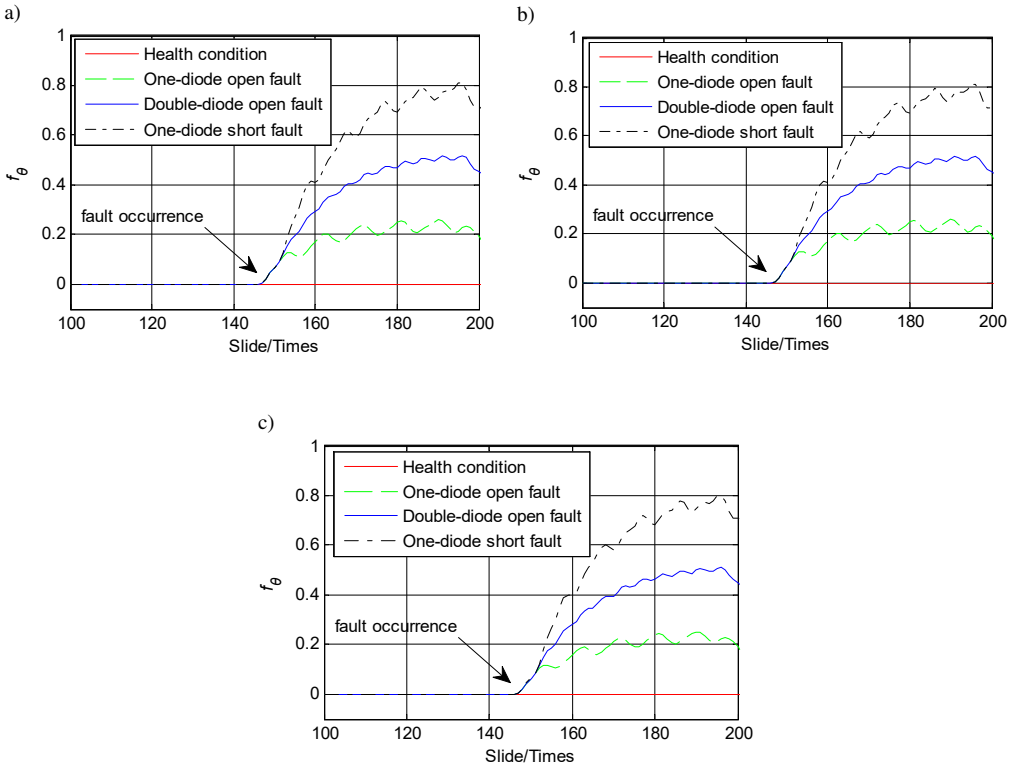

Fig. 9. Change curve of f_θ under different load conditions: (a) no load condition; (b) resistive load condition; (c) resistive-inductive load condition.

3.1.4. Fault diagnosis

Based on the extracted features obtained by using the dynamic FFT, a method of diagnosing AC generator rotating rectifier is proposed. Two diagnosis methods, the ED based and BPNN based, are considered together in this research. The flowchart of both methods is shown in Fig. 10. There are three steps to diagnose the rotating rectifier of an AC generator.

First, three-phase voltages (U_a, U_b and U_c) need to be acquired synchronously. Then, dynamic FFT is employed to extract fault features. Finally, fault diagnosis can be implemented with the extracted fault features. In the ED based method, centroids of the samples need to be calculated. Fault diagnosis of this method consists in matching the minimum values of Euclidean distances. As for the BPNN classifier, samples need to be used for training to achieve proper weights and bias with which, a new sample can be classified to a specific fault mode.

In this simulation experiment, for each fault mode, 150 experimental samples are collected. So, there are total 600 samples under each load condition. Therefore, there are total 1800 samples under three different load conditions. Data samples in this study are processed using MATLAB R2014b software, which runs on a PC with 3.0 GHz CPU and 4 GB RAM, and the operation system is Windows 7.

In this research, for the BPNN, the activation function from the input layer to hidden layer is “tan sig”, and the activation function from the hidden layer to the output layer is “log sig”. The BPNN has a structure of 3-10-4. This means the size of input neurons, hidden neurons and

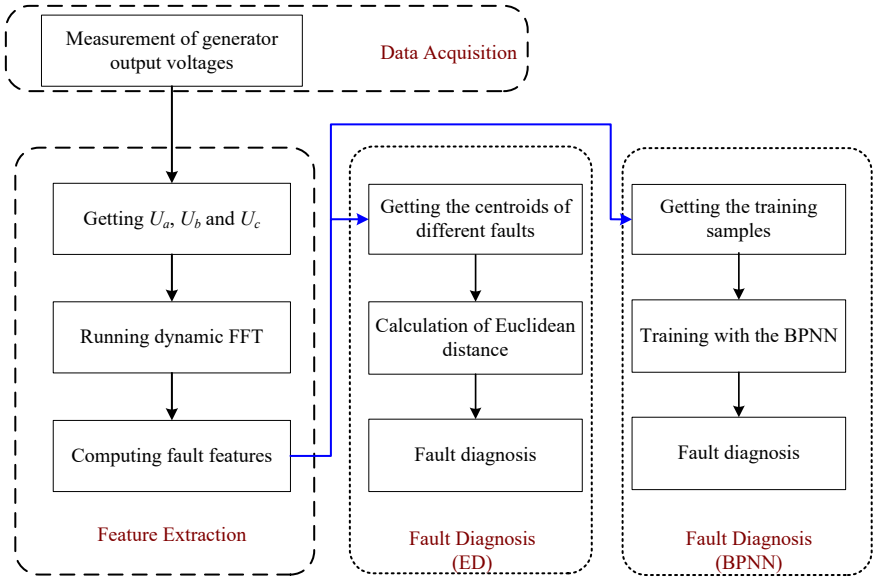

Fig. 10. Flowchart of diagnosis.

output neurons, is set to be 3, 10 and 4, respectively. The learning rate is 0.3. The goal error is set to be 10^{-5}. Also, the BPNN in this research uses 10-fold cross-validation to test the accuracy and stability. The experimental samples are divided into 10 small groups, 9 of which are used as training samples and the remaining group as testing samples. Each test will get the corresponding accuracy. The averaged accuracy of 10 tests is taken as the overall performance of the BPNN. As for the ED method, the ths_0, ths_1 and ths_2, is 0.13, 0.39 and 0.67, respectively.

According to the simulation experiment results, the fault diagnosis accuracy for both methods, can reach the ideal of 100%.

3.2. The second actual experiment

3.2.1. Experiment platform description

Limited by the cost of constructing an aerospace generator, the authors constructed a general civil generator to testify the methods presented above. The civil generator is identical to its aerospace counterparts in terms of structure, and it can be used to testify the effectiveness of the proposed methods. In this real generator system, there is an AVR which calculates the *root-mean-square* (RMS) value of generator main output voltage and compares it with the reference voltage to produce an error which can be used to regulate the exciter current of an AC exciter. In this way, generator output can be controlled with a closed-loop system of excitation voltage regulator. This experimental platform is constructed and shown in Fig. 11.

The platform is mainly composed of a three-stage brushless synchronous generator. An asynchronous induction motor is used as the prime mover to drive the generator, and this motor is controlled with a SIEMENS inverter. Some rated parameters of the induction motor and the generator are described in Table 3. In order to generate the diode open/short fault, the structure of rotating rectifier is modified and open/short faults can be triggered manually with thirteen

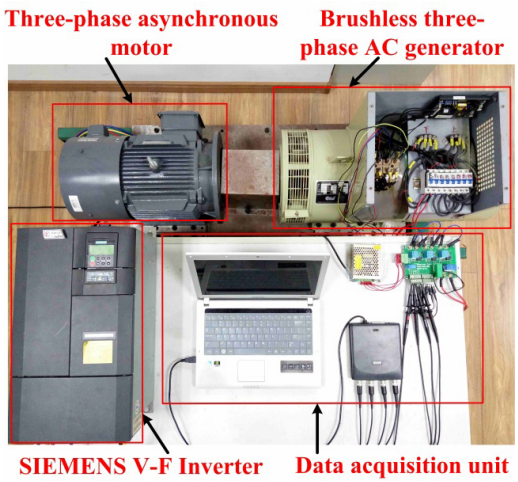

Fig. 11. Experimental platform.

switches, and some of these switches are in series with the corresponding diodes on the rectifier, while others are in parallel with the corresponding diodes. The open/short faults used in this study are identical to those used in the simulation experiment. In this experiment, the resistive load is mainly used for investigation of load variations. Three load conditions are considered: no load, 1.5 kW load and 3 kW load.

Table 3. Parameters of experimental units.

Induction motor		**Three-phase AC generator**	
Parameter	Value	Parameter	Value
Rated power [kW]	11	Rated power [kW]	7.5
Rated voltage [V]	380	Rated speed [rpm]	1500
Rated current [A]	22.5	Rated voltage [V]	220
Rated torque [N.m]	70	Rated frequency [Hz]	50
Number of pole-pairs	2	Pole pairs	2

3.2.2. Data acquisition

In this experiment, output voltages (U_a, U_b and U_c) of the main generator are sampled with a data acquisition system, which is illustrated in Fig. 12. This data acquisition system is composed of an analog signal processing board, a data acquisition unit card (Handyscope HS4 by TiePie Co.) and a *personal computer* (PC). The sampling rate for the data acquisition unit card is set to be 5 KSa/s and each sample contains 1000 data points. For each fault mode, 100 samples are collected and there are 400 samples in total for four fault modes.

Some experimental waveforms of main output voltages under different faults with no load are illustrated in Fig. 13.

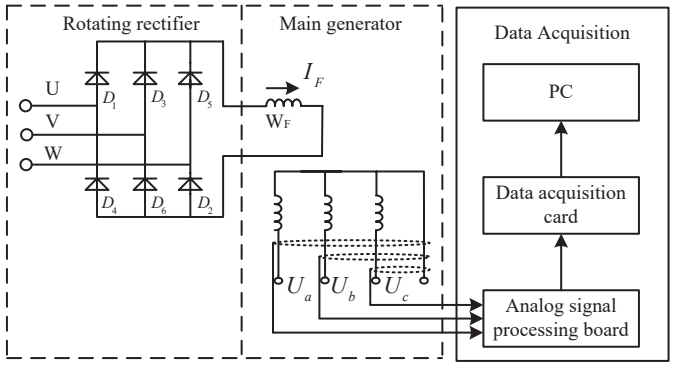

Fig. 12. Data acquisition system.

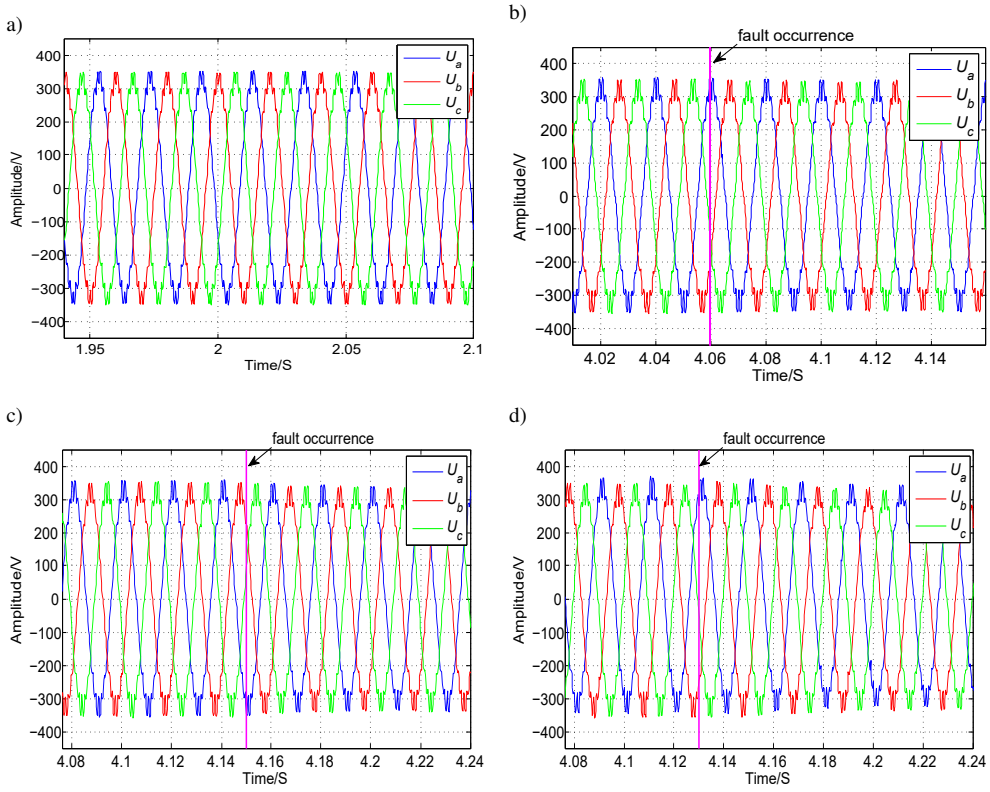

Fig. 13. Experiment waveforms under different faults: (a) working order; (b) D1- open fault ; (c) D1D4 – open fault; (d) D1 – short fault.

3.2.3. Feature extraction

After obtaining the three-phase output voltage signals under three load types: no-load condition, 1.5 kW load condition and 3 kW load condition, the signals are analyzed with the Fourier transform. The input length of the FFT is set as $N_1 = 201$.

Metrol. Meas. Syst., Vol. 28 (2021), No. 2, pp. 269–288
DOI: 10.24425/mms.2021.136607

Figure 14 shows the corresponding spectrum diagrams of U_a when the rotating rectifier is in working order, D1 open circuit fault, D1D4 open circuit fault and D1 short circuit fault under no-load condition, respectively.

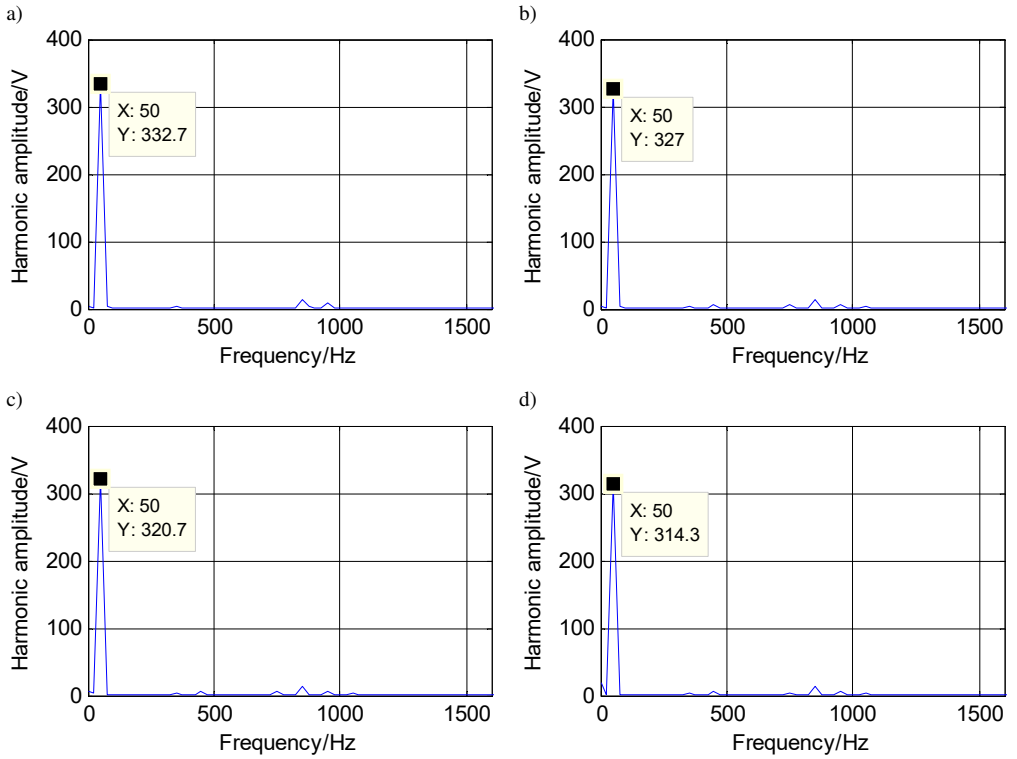

Fig. 14. Spectrum of U_a for different fault modes: (a) working order; (b) D1 – open fault; (c) D1D4 – open fault; (d) D1 – short fault.

In this experiment, the dynamic FFT is applied to the actual samples with the sliding length of 2 points. In this way, 400 instances of sliding FFT processing are carried out, and the f_T feature after each FFT processing is achieved. Under no-load condition, several f_T feature curves can be observed in Fig. 15.

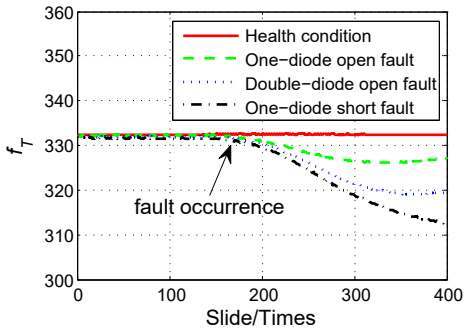

Fig. 15. Change curve of f_T feature under no-load condition.

In the actual experiment, the f_θ features calculated from the f_T curve varies drastically, and this can be attributed to disturbance from the data noise. Hence, a digital filter seems to be necessary. In this research, three filterers, including mean filter, median filter and Kalman filter, are considered and compared in terms of filtering performance. Finally, the Kalman filter method is found to be the most suitable [29]. The f_θ feature curves, before and after Kalman filtering, are shown in Fig. 16, respectively. As can be seen from Fig. 15 and Fig. 16, the results of the actual experiment are similar to those of the simulation experiment.

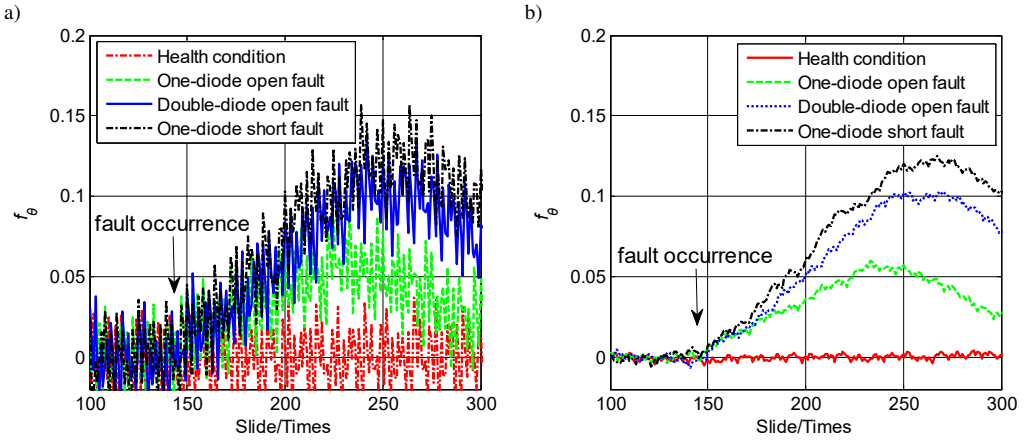

Fig. 16. (a) The curve of f_θ feature before the Kalman filter is applied; (b) The curve of f_θ feature after the Kalman filter is applied.

3.2.4. Fault diagnosis

In this real experiment, for each fault mode, 100 experimental samples are collected. So, there are total 400 samples under each load condition. Therefore, there are total 1200 samples under three different load conditions. In applications, the generator load may fluctuate under different conditions, and in order to be close to real situations, three types of load samples are mixed and used for the variable load condition.

Similar to that used in simulation experiment, the BPNN designed in this real experiment also has a structure of 3-10-4. The first transfer function is a "tan sig" function and the second transfer function, is a "log sig" function. The learning algorithm of the network is gradient descent method, and the learning rate is set to be 0.3. Also, 10-fold cross-validation method is used in this classifier. With these parameters, the BPNN can achieve good performance. As for the ED method, the ths_0, ths_1 and ths_2, is 0.03, 0.08 and 0.11, respectively.

The results of fault diagnosis based on the BPNN (10-fold cross-validation) and Euclidean Distance method are given in Table 4 in which testing time is the time cost for testing one sample and it should be noted here that this is only roughly estimated by the PC.

It can be seen from the table above, both of classification methods have achieved good results. The BPNN classifier, by using the cross-validation strategy, can achieve good diagnosis accuracy under different load conditions. This indicates that the conventional BPNN is a good classifier in our research so long as the network parameters are properly trained. The method based on ED method is simple, but also effective in diagnosing faults, and it can achieve good results even under variable loads. However, the performance of the ED method seems to be inferior to that

Table 4. Results comparison for diagnosis methods.

Load types	Classifier	Accuracy	Testing time
No load	BPNN (cross-validation)	99%	0.03 ms
	ED	99%	< 0.001 ms
1.5 kW	BPNN (cross-validation)	100%	0.03 ms
	ED	97%	< 0.001 ms
3 kW	BPNN (cross-validation)	99%	0.04 ms
	ED	97%	< 0.001 ms
Variable loads	BPNN (cross-validation)	98%	0.03 ms
	ED	93%	< 0.001 ms

of the BPNN in most cases because the neural network is able to learn the samples itself, and through this capability, this classifier can automatically find a good classification hyper-plane in the feature space. Also, the ED method performs the diagnosis task with fixed threshold values and this method cannot achieve good performance for samples disturbed by noise.

Also, the ideal results from the figures and tables above also illustrate that the f_θ features calculated from the f_T, are effective.

4. Conclusions

In this article the authors present a diagnosis method for the rotating rectifier of an aerospace brushless three-phase synchronous generator based on the dynamic FFT, with which, the f_T curve can be achieved and calculated to extract fault feature f_θ. In order to test the effectiveness of this feature, both the ED method and BPNN classifier are adopted. Several conclusions can be drawn according to the descriptions above.

First, output voltages of the main generator are selected as accessible signal sources and the dynamic FFT method applied to this signal is demonstrated to be effective in extracting f_T and f_θ features of the rotating rectifier of a three-phase aerospace AC generator. The simulated and real experiments show that this feature extraction method is robust to the load variations.

Second, the f_θ features selected for different fault modes in this research have good separability because we can achieve good diagnosis accuracy with either the ED method, or the BPNN classifier. Both classifiers belong to the conventional and typical methods in the field of fault diagnosis.

Third, the features from the simulations are different from those in experiments because of the noise effect. Hence, additional measures need to be adopted to eliminate the noise disturbance. In our research, the Kalman filter can fulfil the filtering task with good results.

Finally, the methods used in our research need many calculations, and we conduct the verification of algorithms via a personal computer. The algorithms can be implemented in an embedded system, which is more suitable for online working ordermonitoring of an aerospace generator. These tasks will be envisaged in the next research.

Acknowledgements

This work was supported by the Fundamental Research Funds for the Central Universities (grant no. NS2017019).

References

[1] Madonna, V., Giangrande, P., & Galea, M. (2018). Electrical power generation in aircraft: review, challenges, and opportunities. *IEEE Transactions on Transport Electrification*, *4*(3), 646–659. https://doi.org/10.1109/TTE.2018.2834142

[2] Rosero, J. A., Ortega, J. A., Aldabas, E., & Romeral, L. (2007). Moving towards a more electric aircraft. *IEEE Transactions on Aerospace and Electronic Systems*, *22*(3), 3–9. https://doi.org/10.1109/MAES.2007.340500

[3] Jiang, S. B., Wong, P. K., Guan, R. C., Liang, Y. C., & Li, J. (2019). An Efficient Fault Diagnostic Method for Three-Phase Induction Motors Based on Incremental Broad Learning and Non-Negative Matrix Factorization. *IEEE Access*, *4*, 17780–17790. https://doi.org/10.1109/ACCESS.2019.2895909

[4] Jia, Z., Liu, Z. B., Vong, C. M., & Pecht, M. C. (2019). A Rotating Machinery Fault Diagnosis Method Based on Feature Learning of Thermal Images. *IEEE Access*, *7*, 12348–12359. https://doi.org/10.1109/ACCESS.2019.2893331

[5] Batzel, T. D., & Swanson, D. C. (2009). Prognostic health management of aircraft power generators. *IEEE Transactions on Aerospace and Electronic Systems*, *45*(2), 473–482. https://doi.org/10.1109/TAES.2009.5089535

[6] Batzel, T. D., Swanson, D. C., & Defenbaugh, J. F. (2003). Predictive diagnostics for the main field winding and rotating rectifier assembly in the brushless synchronous generator. *4th IEEE International Symposium on Diagnostics for Electric Machines, Power Electronics and Drives*, USA, 349–354. https://doi.org/10.1109/DEMPED.2003.1234600

[7] Cui, J., Tang, J., Shi, G. & Zhang, Z. (2017). Generator rotating rectifier fault detection method based on stacked auto-encoder. *IEEE Workshop on Electrical Machines Design, Control and Diagnosis (WEMDCD)*, UK, 256–261. https://doi.org/10.1109/WEMDCD.2017.7947756

[8] Cui, J., Shi, G., & Zhang, Z. (2017). Fault detection of aircraft generator rotating rectifier based on SAE and SVDD method. *Prognostics and System Health Management Conference*, China, 1–5. https://doi.org/10.1109/PHM.2017.8079202

[9] Wei, Z., Pang, J., & Sun, C. (2019). Fault diagnosis of rotating rectifier based on waveform distortion and polarity of current. *IEEE Transactions on Industry Applications*, *55*(3), 2356–2367. https://doi.org/10.1109/TIA.2019.2893140

[10] Sun, S., Wu, Y., Cai, W., & Ding, W. (2017). Fault Diagnosis of Rotating Rectifier Based on Harmonic Features. *IOP Conference Series: Materials Science and Engineering*, *199*, 01246. https://doi.org/10.1088/1757-899X/199/1/012146

[11] Zhang, Z., Liu, W., Peng, J., Zhao, D., Meng, T., Pang, J., & Sun, C. (2017). Identification of TBAES rotating diode failure. *IET Electric Power Applications*, *11*(2), 260–271. https://doi.org/10.1049/iet-epa.2016.0468

[12] Bui, H. K., Bracikowski, N., Hecquet, M., Zappellini, K. L., & Ducreux, J. P. (2017). Simulation of a large power brushless synchronous generator (blsg) with a rotating rectifier by a reluctance network for fault analysis and diagnosis. *IEEE Transactions on Industry Applications*, *53*(5), 4327–4337. https://doi.org/10.1109/TIA.2017.2701789

[13] Huang, C., Yuan, H., Ma, Z., Shi, J., Zhou, L., & Guo, Xin. (2015). The Fault Diagnosis of Aircraft Power System Based on Inverse Problem of Fuzzy Optimization. *Journal of Aerospace Engineering*, *25*, 155–175. https://doi.org/10.1177/0954410015603075

[14] Sottile, J., Trutt, F. C., & Leedy, A. W. (2006). Condition Monitoring of brushless three-phase synchronous generators with stator winding or rotor circuit deterioration. *IEEE Transactions on Industry Applications*, *42*(5), 1209–1215. https://doi.org/10.1109/IAS.2001.955747

[15] Wei, Z., Liu, W., Zhang, Z., Jiao, N., Peng, J., & Meng, T. (2018). Rotating rectifier fault detection method of wound-rotor synchronous starter generator with three-phase exciter. *The 4th International Symposium on More Electric Aircraft Technology*, China, 524–528. https://doi.org/10.1049/joe.2018.0038

[16] McArdle, M. G., & Morrow, D. J. (2004). Noninvasive detection of brushless exciter rotating diode failure. *IEEE Transactions on Energy Conversion*, *19*(2), 378–383. https://doi.org/10.1109/TEC.2003.822325

[17] Mohamed, S., Khmais, B., & Abdelkader, C. (2013). Detection of brushless exciter rotating diodes failures by spectral analysis of main output voltage. *International Conference on Electrical Engineering and Software Applications*, Tunisia, 1–6. https://doi.org/10.1109/ICEESA.2013.6578469

[18] Mohamed, S., Khmais, B., Abdelkader, C., & Mohamed, E. (2014). Brushless Three-Phase Synchronous Generator under rotating diode failure conditions. *IEEE Transactions on Energy Conversion*, *29*(3), 594–601. https://doi.org/10.1109/TEC.2014.2312173

[19] Donald, G., Ziang, Z., Constantin, A., & Chang, X. (2009). A neural network based approach for the detection of faults in the brushless excitation of a synchronous motor. *IEEE International Conference on Electro/Information Technology*, Canada, 423–428. https://doi.org/10.1109/EIT.2009.5189654

[20] Rufus, F., Lee, S., Thakker, A., Field, S. A., & Kumbar, N. (2008). Advanced diagnostics of aircraft electrical generators. *SAE International Journal of Aerospace*, *1*(1), 1064–1070. https://doi.org/10.4271/2008-01-2923

[21] Huang, G., Zhu, Q., & Siew, C. (2004). Extreme learning machine: a new learning scheme of feedforward neural networks. *IEEE International Joint Conference on Neural Networks (IEEE Cat. No.04CH37541)*, Canada, 985–990. https://doi.org/10.1109/IJCNN.2004.1380068

[22] Cui, J., & Wang, Y. (2010). A novel approach of analog fault classification using a support vector machines classifier. *Metrology and. Measurement Systems*, *17*(4), 561–582. https://doi.org/10.2478/v10178-010-0046-0

[23] Cui, J., & Wang, Y. (2011). Analog circuit fault classification using improved one-against-one support vector machines. *Metrology and. Measurement Systems*, *18*(4), 569-582. https://doi.org/10.2478/v10178-011-0055-7

[24] Cui, J. (2015). Faults classification of power electronic circuits based on a support vector data description method. *Metrology and. Measurement Systems*, *22*(02), 205–220. https://doi.org/10.1515/mms-2015-0017

[25] He, J., Zhou, Z., Yin, X., & Chen, S. (2000). Using neural networks for fault diagnosis. *Proceedings of the IEEE-INNS-ENNS International Joint Conference on Neural Networks*, USA, California, 217-220. https://doi.org/10.1109/IJCNN.2000.861460

[26] Tantawy, A., Koutsoukos, X., & Biswas, G. (2012). Aircraft Power Generators: Hybrid Modeling and Simulation for Fault Detection. *IEEE Transactions on Aerospace and Electronic Systems*, 48(1), 552–571. https://doi.org/10.1109/TAES.2012.6129655

[27] Dinesh, G., Adithya, B. V., & Vedula, V. (2015). Modeling of a traditional aircraft generator and its sub-systems. *IEEE International Conference on Electrical, Computer and Communication Technologies (ICECCT)*, India. https://doi.org/10.1109/ICECCT.2015.7225936

[28] Nuzzo, S., Galea, M., Gerada, C., & Brown, N. (2018). Analysis, modelling and design considerations for the excitation systems of synchronous generators. *IEEE Transactions on Industrial Electronics*, *65*(4), 2996–3007. https://doi.org/10.1109/tie.2017.2756592

[29] Julier, S. J., & Uhlmann, J. K. (1997). New extension of the Kalman filter to nonlinear systems. *Proceedings of SPIE – The International Society for Optical Engineering*, *3068*, 182–193. https://doi.org/10.1117/12.280797

Sai Feng received the B.S. degree in electronic and information engineering from Civil Aviation University of China, Tianjin, China, in 2017. He is currently working toward the M.S. degree in precision instrument and machinery at Nanjing University of Aeronautics and Astronautics (NUAA), Nanjing, China. His research interests include health monitoring and fault diagnosis.

Jiang Cui received the Ph.D. degree in instrument science and technology from Nanjing University of Aeronautics and Astronautics (NUAA), Nanjing, China, in 2011. He is currently Associate Professor with NUAA, China. He has authored or co-authored one book and over 80 articles. He holds 5 patents. His current research interests include machine learning applications, fault diagnosis and health monitoring of power electronic system with data-driven methods.

Zhuoran Zhang received the Ph.D. degree in electrical engineering from Nanjing University of Aeronautics and Astronautics (NUAA), Nanjing, China, in 2009. He is currently Full Professor in NUAA. From Feb. 2012 to Jun. 2013, he was a visiting professor in Wisconsin Electric Machines and Power Electronics Consortium (WEMPEC), University of Wisconsin-Madison, U.S. He is also an IEEE senior member. His research interests include design and control of electric machines for aircraft power. He has authored or co-authored over 170 technical papers and two books. He holds 36 issued patents in these areas.